

Graphene-Insulator-Superconductor junctions as thermoelectric bolometers

Leonardo Lucchesi and Federico Paolucci

Dipartimento di Fisica, Università di Pisa, Largo Bruno Pontecorvo 3, 56127 Pisa, PI, Italy and INFN Sezione di Pisa, Largo Bruno Pontecorvo 3, 56127 Pisa, PI, Italy

We design a superconducting thermoelectric bolometer made of a Graphene-Insulator-Superconductor tunnel junction. Our detector has the advantage of being passive, as it directly transduces input power to a voltage without the need to modulate an external bias. We characterize the device via numerical simulation of the full nonlinear thermal dynamical model of the junction, considering heating of both sides of the junction. While estimating noise contributions, we found novel expressions due to the temperatures of both sides being different than the bath temperature. Numerical simulations show a Noise Equivalent Power $NEP \sim 4 \times 10^{-17} \text{ W}/\sqrt{\text{Hz}}$ for an input power of $\sim 10^{-16} \text{ W}$, a response time of $\tau_{th} \sim 200 \text{ ns}$ and an integration time to obtain a Signal-to-Noise Ratio $SNR = 1$ of $\tau_{SNR=1} \sim 100 \mu\text{s}$ for an input power $\sim 10^{-13} \text{ W}$. Therefore, the device show promise for large-array cosmological experiment applications, also considering its advantages for fabrication and heat budget.

I. INTRODUCTION

Research on terahertz detection has grown rapidly in recent years due to its relevance in both fundamental science [1, 2] and a wide range of technological applications [3–5]. In this frequency range, thermal detectors such as bolometers become especially important because of the so-called terahertz gap, namely the lack of reliable solid-state devices based on direct photon absorption (see [6] p.55). For Cosmic Microwave Background (CMB) measurements, present requirements for Noise Equivalent Power (NEP) and saturation power typically lie around $NEP \sim 10^{-17} \text{ W}/\sqrt{\text{Hz}}$ and $P_{sat} \sim 10 \text{ pW}$ [7–9], whereas upcoming experiments aim to introduce stricter requirements, with $NEP \sim 3 \cdot 10^{-20} \text{ W}/\sqrt{\text{Hz}}$ and $P_{sat} \sim 0.2 \text{ fW}$ [10]. The Transition-Edge Sensor (TES) remains the benchmark technology for bolometry in astroparticle physics [9, 11], with a measured best performance of $NEP = 3 \times 10^{-19} \text{ W}/\sqrt{\text{Hz}}$ [12]. However, its operation is complicated by the difficulty of DC readout, by the need for biasing electronics, and the heating associated with it [13], while for ground-based experiments the NEP is still limited to $\sim 10^{-17} \text{ W}/\sqrt{\text{Hz}}$ by environmental factors (see [9] and references within).

An alternative approach is offered by Kinetic Inductance Detectors (KIDs), showing a record $NEP \sim 3 \times 10^{-19} \text{ W}/\sqrt{\text{Hz}}$ [14]. They have already been deployed—for example, in the OLIMPO experiment, achieving $NEP = 4.5 \cdot 10^{-17} \text{ W}/\sqrt{\text{Hz}}$ at 150, GHz with an input power of $P = 3 \text{ pW}$ [15]. KIDs alleviate the readout challenges and mitigate heating issues typical of TES-based systems. However, their physics is quite complex, and they require costly electronics and wiring for probe signals. They can absorb photons directly by destroying a Cooper pair, reducing the need for antennas, but only above the superconducting gap $\nu > \Delta$ [16] (for Al, $\nu > 90 \text{ GHz}$), which poses limitations for CMB applications.

Another class of detectors employs Superconducting Tunnel Junctions (STJs). Their working principle relies on

the strong temperature dependence of STJ conductivity, and various junction types have been explored, including metal–insulator–superconductor (NIS) devices used in hot-electron bolometers [17] and cold-electron bolometers [18, 19]. Both these designs require voltage or current biasing, with the same problems mentioned for the other technologies.

A different approach to detection is represented by passive detectors which directly generate the signal from the input power without the need to modulate a bias. A passive detector concept is the superconducting thermoelectric bolometer [13], which measures the thermoelectric current or voltage produced by heating induced by the incident signal. Such a detector could in principle overcome several of the issues described above. Among the possible implementations, STJ-based structures are particularly promising, as strong thermoelectric effects arise in Ferromagnet–Insulator–Superconductor (FIS) junctions [20]. A further mechanism for strong thermoelectricity, accessible in Superconductor–Insulator–Superconductor’ (SIS’) junctions [21], is nonlinear thermoelectricity, obtained by heating the superconductor with the larger Δ . Peculiarly, the induced thermovoltage scales with the superconducting gap Δ rather than with the temperature T_h of the hotter electrode [21]. This enables sizeable thermovoltages even for weak heating, since a small increase in T_h can still drive a signal of order $\sim \Delta$. The main limitation of FIS and SIS’ junctions, however, is the requirement of a strong magnetic field within the junction—needed either to activate thermoelectricity (FIS) or to suppress the Josephson current (SIS’).

In this article, we propose the design of a thermoelectric bolometer made of a Graphene-Insulator-Superconductor (GIS) tunnel junction. There are already several examples of GIS junction-based bolometers in literature [22–24], but they generate signals from the temperature dependence of resistance measured via biasing and not from thermoelectricity generation.

We begin our work by describing the thermal dynamics of the device by using a numerical nonlinear model for thermoelectricity in superconducting junctions introduced in

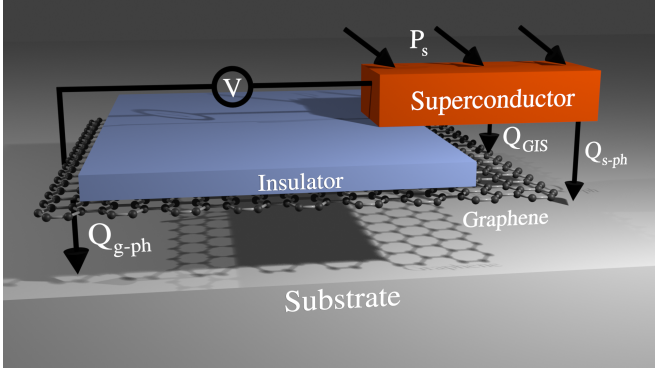


Figure 1. Depiction of the thermoelectric GIS bolometer schematizing its thermal dynamics and the measurement setup.

Ref. [25], and then we discuss the noise sources we considered and how we estimated their contributions to the total noise of the device. Finally, we present the main features and figures of merit of the device, namely the responsivity, the noise equivalent power and the characteristic times.

II. SIGNAL MODEL AND RESULTS

When one side of a GIS junction heats up, a thermoelectric current starts to flow through it [26]. Therefore, we can design a thermal radiation detector by coupling an antenna to one side of the junction and measuring the generated closed-circuit Peltier current I_0 or the open-circuit Seebeck potential V_S . The thermoelectric current or potential generated by the heat carried by the impinging radiation represents the entire signal of our device. Intuitively, this means that we need the largest possible difference between the superconductor temperature T_s and the graphene temperature T_g , thus implying that we will need at least one temperature to be much larger than the bath temperature T_b . As shown in Ref. [25], linear transport models fail to describe the thermal behavior of the system in this regime. Following that discussion, we use the nonlinear numerical model defined in Ref. [25] to describe the junction behavior and estimate the noise performance of the detector. Here, we only summarize its main points.

Current and heat transport across the GIS junction can be described by the usual tunneling formulas [25, 27]

$$I(V, T_s, T_g) = \frac{1}{eR_T} \int dE \rho_s(E, T_s) \cdot \rho_g(E - E_F - eV) [f(E - eV, T_g) - f(E, T_s)], \quad (1)$$

$$Q_{\text{GIS}}(V, T_s, T_g) = \frac{1}{e^2 R_T} \int dE (E - eV) \rho_g(E - E_F - eV) \cdot \rho_s(E, T_s) [f(E, T_s) - f(E - eV, T_g)], \quad (2)$$

where R_T is the tunneling resistance, $f(E, T)$ is the Fermi function, V is the electrostatic potential across the junction, E_F is the Fermi energy, ρ_s and ρ_g are the densities of states (DOSSs) of the superconductor and graphene defined by Eqs. 2c, 4 and 8 of Ref. [25]. We consider here doped graphene with electron density $n_0 = 1 \times 10^{12} \text{ cm}^{-2}$ corresponding to $E_F = 98 \text{ meV}$. The effects of different values of E_F were explored in Ref. [26]. We also choose Al as superconductor, with DOS at the Fermi energy in the metallic state $N_F = 2.15 \times 10^{47} \text{ J}^{-1} \text{ m}^{-3}$ [28], and zero-temperature energy gap $\Delta_0 = 2 \times 10^{-4} \text{ eV}$.

From these expressions, we can obtain $I_0 = I(0, T_s, T_g)$ and V_S by solving $I(V_S, T_s, T_g) = 0$ for any T_s and T_g . In both open and closed-circuit operation, we assume that we have an ideal voltmeter and an ideal ammeter connecting the superconductor and the graphene layers, respectively. Therefore, to compute the response of our device to an input power, we need to describe the thermal dynamics of the junction. Each side of the junction exchanges a power Q_{GIS} with the other side, following Eq. 2, and dissipates a power $Q_{s-\text{ph}}(T_s)$ (Eq. 6 [25]) and $Q_{g-\text{ph}}(T_g)$ (Eq. 7a [25]) through interaction with the phonon gas, which is at the bath temperature T_b if we assume a negligible Kapitza resistance [24]. The physics translates into a system of two coupled nonlinear differential equations for the time-dependent temperatures $T_{s,g}(t)$ that we solve numerically [25]

$$\begin{cases} C_s(T_s) \frac{dT_s}{dt} = -Q_{\text{GIS}}(T_s, T_g) - Q_{s-\text{ph}}(T_s) + P_s \\ C_g(T_g) \frac{dT_g}{dt} = Q_{\text{GIS}}(T_s, T_g) - Q_{g-\text{ph}}(T_g) + P_g, \end{cases} \quad (3)$$

where $C_g(T) = A_g \frac{\pi^2}{3} k_B^2 n_g(E_F) T$ [24] is the thermal capacitance of the graphene layer, with A_g the area of the graphene layer, $n_g(E_F)$ the density of electrons at the Fermi energy, and k_B the Boltzmann constant, and $C_s(T) = T dS_s/dT$ is the thermal capacitance of the superconductor layer, computed from the quasiparticle entropy $S_s(T)$ [29]. $P_{s,g}$ are the external radiant powers impinging on the superconductor and the graphene. We will only explore results with $P_g = 0$ and $P_s \neq 0$, because with $T_g > T_s$ the absence of nonlinear thermoelectricity reduces the signal [25], as also explained below. We will also restrict our analysis to the open-circuit configuration because nonlinear thermoelectricity in this system induces relatively larger V_S than I_0 [25].

For a bolometer, we can assume that the variation of P_s is slower than the system response time τ_{th} (and we will later prove that τ_{th} is reasonably small enough), allowing us to use the steady-state values $T_s(t \rightarrow \infty) \equiv T_s$ and $T_g(t \rightarrow \infty) \equiv T_g$ to compute all physical quantities. We numerically solve Eq. 3 for different T_b to obtain the dependence of T_s and T_g on P_s , shown in Fig. 2a). As we can see from the plot, δT is monotonic in P_s , but the dependence is not linear as predicted by linear models [13], even for very small P_s [25]. We can also notice the effect of the difference in T_b vanishing for larger P_s , where dissipation processes dominate the thermal dynamics of the system.

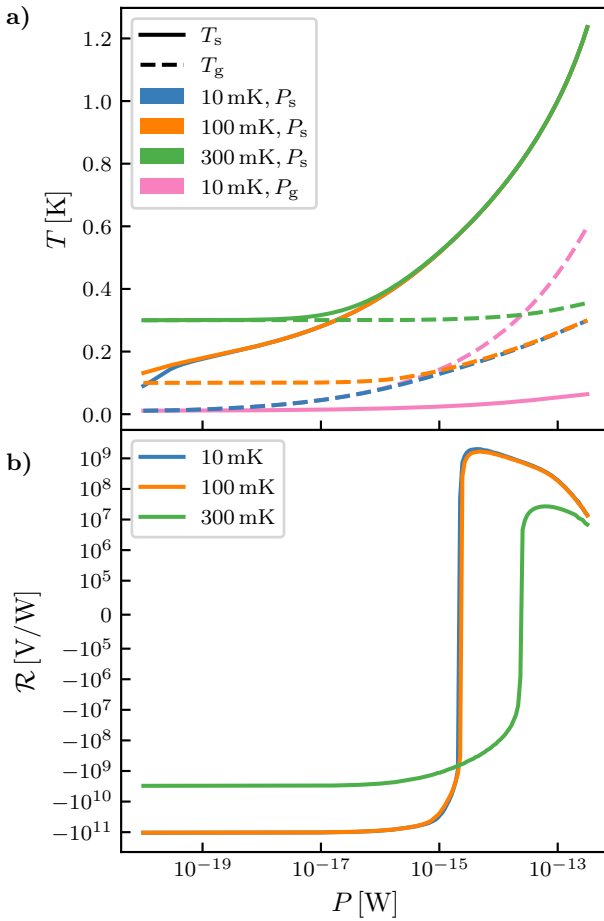


Figure 2. Device response to steady input power P . a) Dependence on P of superconductor and graphene temperatures T_s, T_g for different T_b and antenna placement. Temperature are reasonably smooth in every case, with converging T_s for larger P . Connecting the antenna to graphene reduces the thermal gradient. b) Responsivity \mathcal{R} dependence on P for different T_b with antenna on superconductor. \mathcal{R} shows large negative values for small P , then becomes positive passing from zero. This is due to a saturation effect described in the main text and in Ref. [25].

We choose a specific geometry with $A_g = 100 \mu\text{m}^2$, a superconductor volume of $V_s = 0.5 \times 10^{-3} \mu\text{m}^3$, and overlap area $A_j = 0.01 \mu\text{m}^2$ because this geometry allows the formation of the largest thermal gradient $\delta T = T_s - T_g$ and gives the best results in terms of signal and noise. Some effects of different geometries are analyzed in Ref. [25]. We will use this geometry from now on.

The most representative figure of merit for the signal is the responsivity $\mathcal{R} \equiv \delta V_s / \delta P_s$, defined as the variation in the signal (in open-circuit δV_s) induced by a small variation in the input power δP_s . Since we consider this small variation to happen over a background power P_s , we can compute the system behavior by linearizing Eq.3 around the steady-state solutions $\{T_s(P_s), T_g(P_s)\}$. Af-

ter a Fourier transform $t \rightarrow \omega$, we can describe the system's linear response $\{\delta T_s, \delta T_g\}$ around a point $\{T_s, T_g\}$ to power oscillations $\delta P_s(\omega)$ and $\delta P_g(\omega)$ by linearizing Eq.3 as

$$\begin{cases} i\omega C_s \delta T_s = - \left(\frac{\partial Q_{\text{GIS}}}{\partial T_s} + \frac{\partial Q_{s-\text{ph}}}{\partial T_s} \right) \delta T_s - \frac{\partial Q_{\text{GIS}}}{\partial T_g} \delta T_g + \delta P_s \\ i\omega C_g \delta T_g = \left(\frac{\partial Q_{\text{GIS}}}{\partial T_g} - \frac{\partial Q_{g-\text{ph}}}{\partial T_g} \right) \delta T_g + \frac{\partial Q_{\text{GIS}}}{\partial T_s} \delta T_s + \delta P_g. \end{cases} \quad (4)$$

By using the linearized thermal dynamics, we can describe the linear variation of the signal δV_s in terms of the linear response functions $\Theta_{gs}(T_s, T_g, \omega) \equiv \delta T_g / \delta T_s$ and $\Theta_{sp}(T_s, T_g, \omega) \equiv \delta T_s / \delta P_s$ (expressions in Appendix), obtaining

$$\mathcal{R} = \left(\frac{\partial V_s}{\partial T_s} + \frac{\partial V_s}{\partial T_g} \Theta_{gs} \right) \Theta_{sp}, \quad (5)$$

where we compute the derivatives of V_s from numerically computing V_s on a (T_s, T_g) grid [25]. We show that the dependence of \mathcal{R} on P_s in Fig.2b). \mathcal{R} assumes very large negative values $\sim -10^{11} \text{ V/W}$ for low powers up to $P_s \sim 1 \text{ fW}$. For powers larger than $P_s \sim 1 \text{ fW}$, \mathcal{R} inverts its sign and reaches relatively large positive values $\mathcal{R} \sim 10^9 \text{ V/W}$. This sign inversion is a nonlinear effect, described in Ref. [25], due to the fact that for larger powers, $V_s(P_s)$ is not a monotonic function [25]. Intuitively, for larger P_s , the dominant contribution to changes in V_s is caused by the change in T_g and not by the change in T_s . This results in an inverted behavior, as an increase in P_s implies an increase in T_g , reducing the thermal gradient and thus the absolute value of V_s .

This zeroes in \mathcal{R} have unfavourable implications in the noise figures of merit, as we will see below. However, the system can be used as a bolometer in both regimes as long as the power is far enough from the inversion point where $\mathcal{R} = 0$.

III. NOISE MODEL AND RESULTS

To assess device properties, modeling noise has the same importance as modeling the signal. While physical noise sources are the same at room temperature and at cryogenic temperature, dominant contributions dramatically change for temperatures lower than the Bloch-Grüneisen temperature [17, 24, 30, 31]. As stated above, we focus on the open-circuit configuration.

Noise registered in the measurement comes from charge and energy fluctuations in the quasiparticle gases on both sides of the junction. Charge fluctuations are directly measured via the induced potential fluctuations δV_s , while the effect of energy fluctuations on steady-state temperatures can be described via Eq. A1, if the variation is slow enough ($\omega \ll 1/\tau_{\text{tun}}$, where $\tau_{\text{tun}} = e/I \sim 10^{-9} \text{ s}$ is the average time between electron tunneling events).

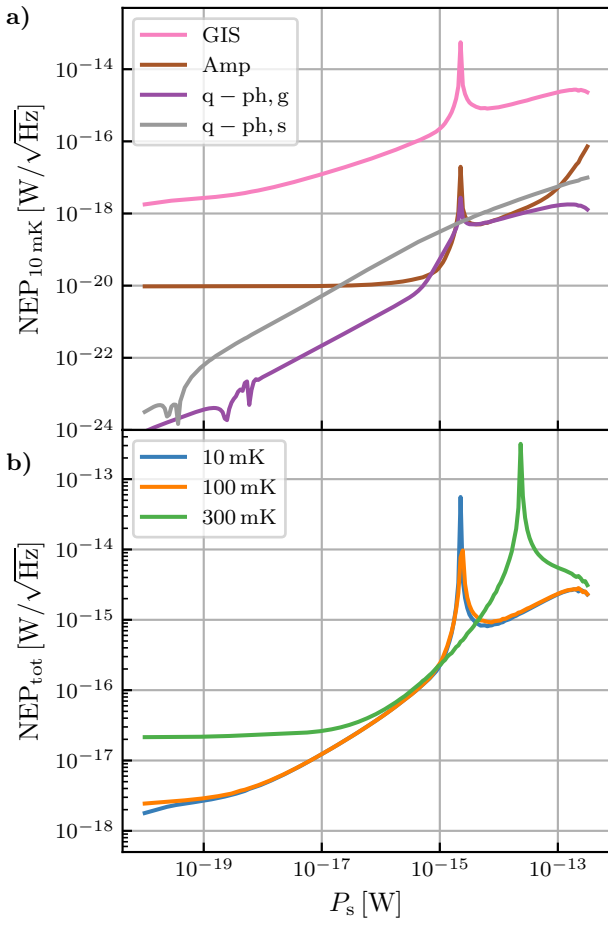


Figure 3. Partial and total NEP dependence on P_s . a) NEP contribution at $T_b = 10$ mK for each noise source. Junction noise dominates by several orders of magnitude because of large dynamical resistance R_d . The peak represents the zero of the responsivity \mathcal{R} . b) Comparison between total NEP dependences on P_s for different T_b . The best reasonable value for the NEP is $4 \times 10^{-17} \text{ W}/\sqrt{\text{Hz}}$ for $P_s \sim 10^{-16} \text{ W}$ for $T_b = 100$ mK, but the choice for T_b could depend on the required input power for the device.

We can compare the effects of very different noise contributions by showing their Noise Equivalent Power (NEP), an important bolometric figure of merit [13, 17] defined as the input power δP_s required to generate a signal equal to the average value of the noise δV_s with a 1 Hz sampling interval. Following standard literature [17, 24], we now describe how we estimate the NEP for each dominant noise contribution before computing the total NEP by quadrature sum of all contributions [32].

a. *Johnson-Nyquist noise* Any resistive element with resistance R in a circuit induces an open-circuit voltage noise $\langle \delta V^2 \rangle = 4k_B R T \delta\omega$ [33]. With our geometry, the graphene layer induces a voltage noise of $\delta V_g \equiv \sqrt{\langle \delta V^2 \rangle} \sim 5.9 \times 10^{-10} \text{ V}/\sqrt{\text{Hz}}$ at $T_g = 1 \text{ K}$ if we assume a graphene mobility of $\mu_g = 10^3 \text{ cm}^2/\text{V}\cdot\text{s}$ and

a carrier density $n_0 = 10^{12} \text{ cm}^{-2}$. However, this noise has to be summed incoherently with the noise from the amplifier circuit required to read V_s , that we can estimate to be $\delta V_{\text{Amp}} \sim 10^{-9} \text{ V}/\sqrt{\text{Hz}}$ [34]. Therefore, we only keep δV_{Amp} for estimation purposes. We can then compute the corresponding NEP by using the definition of responsivity $\text{NEP}_{\text{Amp}} = \delta V_{\text{Amp}}/\mathcal{R}$ [17].

b. *Phonon noise* The interaction between quasiparticles and phonons induces energy fluctuations in a quasi-particle gas [30, 32, 35]. These fluctuations happen in both the superconductor and the graphene layer, and they respectively depend on T_s and T_g . We assume a negligible Kapitza resistance, therefore we consider the phonon gas to be at the thermal bath temperature T_b . For the superconductor layer, we estimate the phonon noise power spectral density by using the equilibrium formula $\delta P_{\text{q-ph,s}}^2 = 4k_B G_{\text{q-ph,s}} T_s^2 \delta\omega$ [17, 30, 35], with the quasiparticle-phonon thermal conductivity defined as $G_{\text{q-ph,s}} = \partial Q_{\text{s-ph}}/\partial T_s$. Even if the quasiparticles and the phonons are not at equilibrium when $T_s \neq T_b$, we believe this formula to be a cautious approximation because it corresponds to considering the phonon gas to be at the same temperature as the quasiparticle gas, therefore inducing a larger number of interactions and thus strongly overestimating noise. This noise induces power fluctuations $\delta P_{\text{q-ph,s}}$ in the superconductor gas, and therefore it adds to the signal P_s , thus implying $\text{NEP}_{\text{q-ph,s}} = \delta P_{\text{q-ph,s}}$.

For the graphene layer, we estimate the phonon noise power spectral density by using the Eq. 42 from [24], with $\delta = 4$, $\delta P_{\text{q-ph,g}}^2 = 8k_B A_g \Sigma_C (T_g^5 + T_b^5)$, where Σ_C is obtained in Eq. 13 of the same article. This noise acts as an oscillating δP_g in the second line of Eq. A1. This means that it does not generate a δV_s with the same mechanism as a δP_s oscillation, and that we cannot equate the NEP to $\delta P_{\text{q-ph,g}}$, and we need to compute the response function $\mathcal{R}_g \equiv \delta V_s/\delta P_g$ and translate the δV_s oscillation back to an equivalent input power fluctuation $\delta V_s/\mathcal{R} \equiv \text{NEP}$, which is the NEP by definition. After algebraic manipulation of Eq. A1, we obtain

$$\mathcal{R}_g = \left[\frac{\partial V_s}{\partial T_g} \left(1 - \frac{\partial Q_{\text{GIS}}}{\partial T_g} \Theta_{gs} \right) - \frac{\partial V_s}{\partial T_s} \frac{\partial Q_{\text{GIS}}}{\partial T_g} \Theta_{sp} \right] \mathcal{K}_g, \quad (6)$$

where the expression for $\mathcal{K}_g(T_s, T_g, \omega)$ can be found in the Appendix. We can then compute $\text{NEP}_{\text{q-ph,g}} = (\mathcal{R}_g/\mathcal{R}) \delta P_g$.

c. *Junction noise* The stochasticity of the tunneling process implies that the amount of charge and energy flowing through the junction fluctuates [30, 36]. We estimate the contribution to the total NEP by using the fluctuations in current $\langle \delta I^2 \rangle$, power $\langle \delta P_j^2 \rangle$ and their cross correlation $\langle \delta P_j \delta I \rangle$ from Eqs. 38, 39, 40 of [24], computed from the statistical fluctuations in the number of tunneling quasiparticles by weighing the fluctuations on charge and energies [17, 30].

Similarly to $\text{NEP}_{\text{q-ph,g}}$, δP_j does not simply enter Eq. A1 as a δP_s oscillation, but rather it acts as a simultaneous power oscillation on both sides $\delta P_g = -\delta P_s = \delta P_j$

because of energy conservation. We use algebra analogous to Eq. 6 to compute the response function $\mathcal{R}_{P_j} \equiv \delta V_S / \delta P_j$, obtaining

$$\begin{aligned} \mathcal{R}_{P_j} = & -\frac{\partial V_S}{\partial T_s} \left(\frac{\partial Q_{\text{GIS}}}{\partial T_g} \mathcal{K}_g + 1 \right) \Theta_{sp} + \\ & + \frac{\partial V_S}{\partial T_g} \left[\mathcal{K}_g - \Theta_{gs} \Theta_{sp} \left(\frac{\partial Q_{\text{GIS}}}{\partial T_g} \mathcal{K}_g + 1 \right) \right]. \end{aligned} \quad (7)$$

While we compute the function for the case $P_g = 0, P_s \neq 0$, we can find analogous functions for different device configurations.

We estimate the open-circuit voltage noise from current fluctuations by using the standard formula $\delta V_I = (dI/dV)^{-1} \delta I \equiv R_d \delta I$ [17, 30, 36], where we use the derivative of Eq. 1. Considering that we can use the same rules for the cross-correlation [17], the final result for the NEP corresponding to junction noise is

$$\text{NEP}_j^2 = \frac{\mathcal{R}_{P_j}^2 \langle \delta P_j^2 \rangle + R_d^2 \langle \delta I^2 \rangle - 2 \mathcal{R}_{P_j} R_d \langle \delta P_j \delta I \rangle}{\mathcal{R}^2}, \quad (8)$$

where the relative sign between the correlation and the squared noise contributions comes from the tunneling process properties [30].

In Fig. 3a, we can see the results for every NEP contribution computed for our device setup with $T_b = 10 \text{ mK}$. We can see that the junction contribution overwhelmingly dominates over every other noise source. This is mainly due to the large contribution of the $\langle \delta I^2 \rangle$ part, which is multiplied by a large dynamic resistance $R_d \sim 1 \text{ G}\Omega$. This large R_d comes from the junction still being away from the Ohmic part of the IV curve at $V = V_S$ for our values of the Seebeck potential. The sharp peaks present in each contribution except $\text{NEP}_{q-ph,s}$ correspond with the $\mathcal{R} = 0$ point shown in Fig. 2b.

In Fig. 3b, we represent the total NEP dependence on input power P_s for different values of T_b . This is the most important figure of merit for a bolometer, and for our setup its most useful value is $\text{NEP}_{100 \text{ mK}} \sim 4 \times 10^{-17} \text{ W}/\sqrt{\text{Hz}}$ estimated for $P_s \sim 10^{-16} \text{ W}$ and $T_b = 100 \text{ mK}$, since it shows similar behavior to 10 mK. Another important feature is that, for intermediate powers $10^{-16} \text{ W} \lesssim P_s \lesssim 10^{-14} \text{ W}$, the larger bath temperature $T_b = 300 \text{ mK}$ shows a performance similar to the smaller T_b , useful for further relaxing requirements on the cryogenic apparatus.

IV. CHARACTERISTIC TIMES

Characteristic times represent another important consideration for a bolometer design. The two most important timescales to represent the behavior of the bolometer are the response time and the integration time needed to obtain a useful measurement.

Since electrical response times are much faster, we estimate the bolometer response time via the thermal re-

sponse time τ_{th} , the time needed by the system to adjust its temperature after a change in the power input. We imagine a response to a small variation δP over a larger power input P_s , that makes the system reach a new steady state exponentially via Eq. 3, with a characteristic time

$$\tau_{th} = \frac{C_s(T_s)}{G_{\text{GIS}}(T_s, T_g) + G_{q-ph,s}(T_s)}, \quad (9)$$

where $G_i = \partial Q_i / \partial T_s$. This standard approximation [32, 35] is reasonable for estimation purposes, and it gives a correct physical picture for experiments where the signal variations are rather slow, such as the sky scans for CMB survey.. We represent the dependence of τ_{th} on P_s in Fig. 4a. For smaller $P_s < 10^{-17} \text{ W}$, τ_{th} is constant for $T_b = 10, 100 \text{ mK}$, then it drops down by an order of magnitude from $P_s \sim 10^{-17} \text{ W}$ to $P_s \sim 10^{-13} \text{ W}$. For $T_b = 300 \text{ mK}$, τ_{th} is almost constant. For $T_b = 300 \text{ mK}$, τ_{th} shows the same behavior as $T_b = 100 \text{ mK}$, except for a different limit value at lower P_s , due to non-negligible quasiparticle dissipation in the superconductor (see Fig. 4 in Ref. [25]). We proved in the Appendix that, for small P_s , τ_{th} converges to a fixed value $\tau_0 = \mathcal{V}_s N_F e^2 R_T \simeq 2.76 \mu\text{s}$, as long as $G_{q-ph,s} \ll G_{\text{GIS}}$ $T_g \ll T_s$ and $T_s \ll \Delta_0/k_B$. In Fig. 4 of [25], we can see that $Q_{s-ph,s}$ is very small for $T_s \lesssim 0.3 \text{ K}$, and thus $G_{q-ph,s}$ is negligible except for $T_b = 300 \text{ mK}$. We can see that τ_{th} reaches $\sim 200 \text{ ns}$ for $P_s \sim 10^{-13} \text{ W}$. The effect of $G_{q-ph,s}$ also inverts the dependence of τ_{th} on P_s , making it drop, while G_j alone would make it rise.

We define the integration time

$$\tau_{\text{SNR}=1} = \frac{1}{2} \left(\frac{\text{NEP}_{\text{tot}}}{P_s} \right)^2 \quad (10)$$

as the time that a signal of fixed power P_s needs to be integrated to have a signal-to-noise ratio $\text{SNR} = 1$. Integrating for a longer time reduces the frequency interval, and thus reduces the absolute value of the noise power. In Fig. 4b, we show the dependence of $\tau_{\text{SNR}=1}$ on P_s . Interestingly, $\tau_{\text{SNR}=1}$ becomes smaller with P_s , down to $\sim 100 \mu\text{s}$ for $P_s \sim 10^{-13} \text{ W}$. The $\mathcal{R} = 0$ peaks are present also in this plot, due to the NEP at the numerator.

V. CONCLUSIONS

Throughout this article, we have proposed and numerically characterised a thermoelectric bolometer made of a Graphene-Insulator-Superconductor junction. After assessing that we have a better device performance by mounting the antenna on the superconductor side, we discovered that the device shows a large responsivity \mathcal{R} up to $|\mathcal{R}| \sim 10^{11} \text{ V/W}$ for $P_s \lesssim 1 \text{ fW}$ and $T_b = 100 \text{ mK}$. Furthermore, our device design shows a $\text{NEP} \sim 4 \times 10^{-17} \text{ W}/\sqrt{\text{Hz}}$ for $P_s \sim 10^{-16} \text{ W}$ and $T_b = 100 \text{ mK}$, and a $\text{NEP} \sim 2 \times 10^{-15} \text{ W}/\sqrt{\text{Hz}}$ for

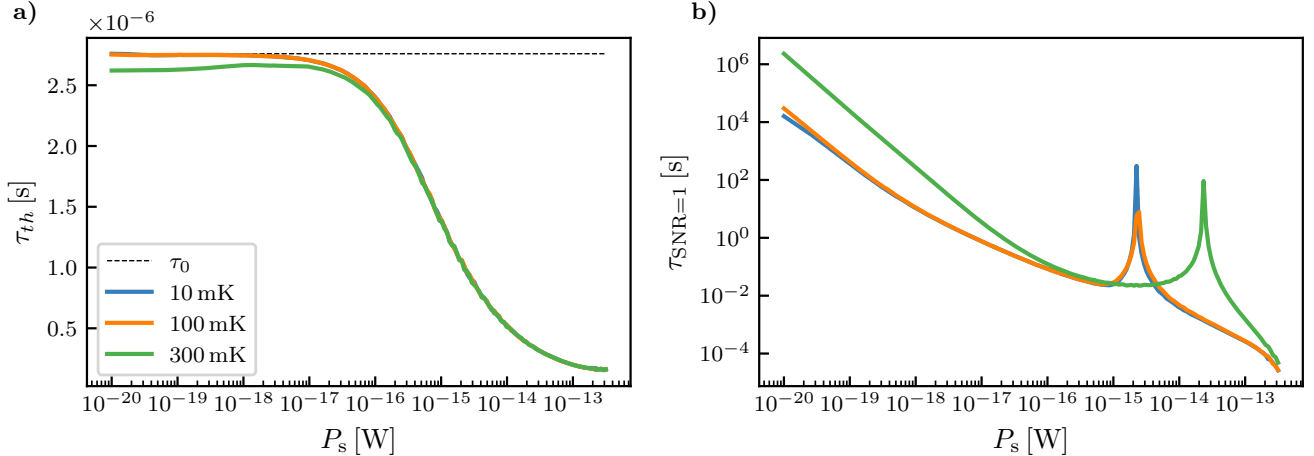


Figure 4. Characteristic times dependence on P_s . a) Thermal response time τ_{th} for different T_b . The curves for 10 and 100 mK are almost identical. For small P_s and T_b , $\tau_{th}(P_s) \simeq \tau_0$ shows almost no temperature dependence (see main text). τ_{th} drops for larger P_s because of increased energy dissipation in the superconductor. b) Integration time necessary to get a signal-to-noise-ratio equal to 1 $\tau_{SNR=1}$. While our bolometer shows very large integration times $\sim 10^3$ s for smaller powers, the integration time improves with P_s , dropping down to ~ 1 ms for $P_s \sim 10^{-13}$ W and $T_b = 100$ mK. Integration times are computed for signal variations corresponding to the entire signal.

$P_s \sim 10^{-13}$ W. Even if our NEP is larger than the measured $\sim 10^{-17}$ W/ $\sqrt{\text{Hz}}$ found in literature [9] and the requirement for future experiments, it is a passive detector design with performance almost comparable with active detectors. In the preparation of a large array experiment, a smaller impact on the heat budget and cheaper fabrication could be more useful than a smaller NEP, that can in principle be compensated by longer integration times. Since this is a preliminary study, further optimization could also improve the noise performance of our device. Our detector shows response times down to $\tau_{th} \sim 200$ ns for $P_s \sim 10^{-13}$ W, and integration times down to $\tau_{SNR=1} \sim 100$ μ s for $P_s \sim 10^{-13}$ W. These values are compatible with investigations of signals arising from experiments focused on interesting physical phenomena, such as the polarization of cosmic microwave background [7]. Thus, this technology might be implemented in experiments where the total power budget of the apparatus is limited, such as balloon or satellite based cosmology experiments.

ACKNOWLEDGMENTS

The authors wish to thank T.T. Heikkilä for fruitful discussion. The Italian Ministry of University and Research partially funded the work of L.L. and F.P. under the call PRIN2022 (Financed by the European Union – Next Generation EU) project EQUATE (Grant No. 2022Z7RHRS) and under the call FIS2 project QuLEAP (Grant No. FIS2023-00227). F.P. acknowledges the CSN V of INFN under the technology innovation grant STEEP for partial financial support.

Appendix A: Response functions and linearization of thermal dynamics

To obtain the response functions to small oscillations in input power, we start from the linearized version of the thermal dynamics equations

$$\begin{cases} i\omega C_s \delta T_s = - \left(\frac{\partial Q_{\text{GIS}}}{\partial T_s} + \frac{\partial Q_{\text{s-ph}}}{\partial T_s} \right) \delta T_s - \frac{\partial Q_{\text{GIS}}}{\partial T_g} \delta T_g + \delta P_s \\ i\omega C_g \delta T_g = \left(\frac{\partial Q_{\text{GIS}}}{\partial T_g} - \frac{\partial Q_{\text{g-ph}}}{\partial T_g} \right) \delta T_g + \frac{\partial Q_{\text{GIS}}}{\partial T_s} \delta T_s + \delta P_g. \end{cases} \quad (\text{A1})$$

If we want to understand the response to a variation in δP_s , we algebraically solve the system first for δT_g , obtaining

$$\delta T_g = \Theta_{gs} \delta T_s, \quad (\text{A2})$$

and then we solve for δT_s , obtaining

$$\delta T_s = \Theta_{sp} \delta P_s, \quad (\text{A3})$$

with

$$\Theta_{gs}(T_s, T_g, \omega) \equiv \frac{\delta T_g}{\delta T_s} = \frac{\frac{\partial Q_{\text{GIS}}}{\partial T_s}}{i\omega C_g - \frac{\partial Q_{\text{GIS}}}{\partial T_g} + \frac{dQ_{\text{g-ph}}}{dT_g}} \quad (\text{A4a})$$

$$\Theta_{sp}(T_s, T_g, \omega) \equiv \frac{\delta T_s}{\delta P_s} = \frac{1}{i\omega C_s - \frac{\partial Q_{\text{GIS}}}{\partial T_g} \Theta_{gs}(T_s, T_g, \omega) - \frac{\partial Q_{\text{GIS}}}{\partial T_s} + \frac{dQ_{\text{s-ph}}}{dT_s}}. \quad (\text{A4b})$$

The same set of equations could be solved differently to obtain the response to a small δP_g with a fixed P_s . In that case, we still solve first for δT_g , but this time we obtain

$$\delta T_g = \Theta_{gs} \delta T_s + \mathcal{K}_g \delta P_g, \quad (\text{A5})$$

with

$$\mathcal{K}_g(T_s, T_g, \omega) = \frac{1}{i\omega C_g - \frac{\partial Q_{\text{GIS}}}{\partial T_g} + \frac{dQ_{\text{g-ph}}}{dT_g}}. \quad (\text{A6})$$

The second part is the same as before, and it allows us to find the response functions to power fluctuations in the graphene quasiparticle gas \mathcal{R}_g and to the tunneling-induced power fluctuations in the junction \mathcal{R}_{P_j} , as described in the main text.

Appendix B: Demonstration of constant thermal response time for small input powers

In Fig.4b) of the main text, we can see that for low input powers P_s and low bath temperatures T_b the response time is almost constant. The thermal response time of a bolometer is usually defined as [32]

$$\tau_{th} = \frac{C_{th}}{G_{th}}, \quad (\text{B1})$$

where C_{th} is the thermal capacitance of the active region and G_{th} is the thermal conductance between the charge carriers in the active region and the thermal bath. In the linear regime, C_{th} and G_{th} are computed at the bath temperature, therefore they are constant for every input power. However, as shown in [25], the linear regime breaks for power much smaller than the $P_s \sim 10^{-17} \text{ W}$ where we still observe an almost constant τ_{th} . Here, we prove that the constant value of τ_{th} holds even in the nonlinear regime, as long as T_s and T_g are small enough.

When P_s is small, the bottleneck for heat conduction is the junction G_{GIS} , as phonon-induced dissipation in the superconductor is negligible and phonon-induced dissipation in graphene is strong enough to keep $T_g \sim T_b$. Therefore,

the thermal capacitance of the superconductor acts as the thermal capacitance of the entire system, and the Seebeck potential is negligible $V_S \simeq 0$. From the definitions we obtain

$$C_s(T_s) = T_s \frac{dS_s}{dT_s} = -2\mathcal{V}_s N_F k_B T_s \frac{d}{dT_s} \int_{-\infty}^{+\infty} dE \rho_s(E) f(E, T_s) \log f(E, T_s) \quad (B2)$$

$$G_{\text{GIS}}(T_s, T_g) = \frac{\partial Q_{\text{GIS}}}{\partial T_s} = \frac{1}{e^2 R_t} \frac{\partial}{\partial T_s} \int dE E \rho_g(E - E_F) \rho_s(E) [f(E, T_g) - f(E, T_s)], \quad (B3)$$

where R_T is the tunneling resistance, $f(E, T)$ is the Fermi function, ρ_s and ρ_g are the densities of states (DOSs) of the superconductor and graphene defined by Eqs. 2c, 4 and 8 of Ref. [25], $N_F = 2.15 \times 10^{47} \text{ J}^{-1} \text{ m}^{-3}$ is the superconductor DOS at the Fermi energy in the metallic state, and \mathcal{V}_s is the supeconductor volume. Since we consider doped graphene with electron density $n_0 = 1 \times 10^{12} \text{ cm}^{-2}$, we can assume the relative graphene DOS $\rho_g(E - E_F) = 1$ to be approximately constant over the relevant energy interval and we consider T_s to be low enough to not impact on the superconductor DOS ρ_s .

If we focus on the T_s dependent part of $C_s(T_s)$, we can see that Eq. B2 can be rewritten as

$$\begin{aligned} T_s \frac{d}{dT_s} \int dE \rho_s(E) f(E, T_s) \log f(E, T_s) = \\ T_s \int dE \frac{\partial \rho_s}{\partial T_s} f \log f + \rho_s \frac{\partial f}{\partial T_s} \log f + \rho_s \frac{\partial f}{\partial T_s}. \end{aligned} \quad (B4)$$

The last term in Eq. B4 is zero because $\rho_s(E)$ is even in E and $\partial f / \partial T_s$ is odd in E . In the $T_s \rightarrow 0$ limit ($T_s \ll \Delta_0 / k_B$), we can recast the second term as

$$\lim_{T_s \rightarrow 0} \ln f = \begin{cases} -\frac{E}{k_B T_s} & E > 0 \\ 0 & E < 0 \end{cases} \quad (B5)$$

obtaining

$$\lim_{T_s \rightarrow 0} C_s(T_s) = 2\mathcal{V}_s N_F \int_0^{+\infty} dE E \left(\frac{\partial \rho_s}{\partial T_s} f + \rho_s \frac{\partial f}{\partial T_s} \right). \quad (B6)$$

We now focus on the T_s dependent part of G_{GIS} in Eq. B3,

$$\frac{\partial}{\partial T_s} \int_{-\infty}^{+\infty} dE E \rho_s(E) [f(E, T_s) - f(E, T_g)] = \quad (B7)$$

$$\int_{-\infty}^{+\infty} dE E \left[\frac{\partial \rho_s}{\partial T_s} (f(E, T_s) - f(E, T_g)) + \rho_s \frac{\partial f}{\partial T_s} \right]. \quad (B8)$$

The second term is even in E , and its integral between $-\infty$ and $+\infty$ is just two times its integral between 0 and $+\infty$. If $T_g \ll T_s$,

$$\lim_{T_g \ll T_s} f(E, T_s) - f(E, T_g) = \begin{cases} f(E, T_s) & E > 0 \\ f(E, T_s) - 1 & E < 0. \end{cases} \quad (B9)$$

Then, we can recast the negative energy part of the integral by using the variable transformation $E \rightarrow -E$ and the fact that $\partial \rho_s / \partial T_s$ is an even function of E

$$\int_{-\infty}^0 dE E \frac{\partial \rho_s}{\partial T_s} (f(E, T_s) - 1) = \int_0^{+\infty} dE E \frac{\partial \rho_s}{\partial T_s} f(E, T_s), \quad (B10)$$

which is equal to the positive energy part. Therefore

$$\lim_{T_g \ll T_s} G_j = \frac{2}{e^2 R_T} \int_0^{+\infty} dE E \left(\frac{\partial \rho_s}{\partial T_s} f + \rho_s \frac{\partial f}{\partial T_s} \right). \quad (B11)$$

The T_s dependent parts of C_s and G_j are equal, so if $T_s \rightarrow 0$ and $T_g \ll T_s$, τ_{th} remains constant at the limiting value

$$\lim_{T_g \ll T_s \rightarrow 0} \frac{C_s}{G_j} = \mathcal{V}_s N_F e^2 R_T \simeq 2.76 \mu\text{s}. \quad (B12)$$

In our setup, T_s and T_g follow the conditions even for $P_s > 10^{-17}$ W, but the thermal conductivity induced by quasiparticle-phonon dissipation in the superconductor for $P_s > 10^{-17}$ W is not negligible anymore, inducing the change in τ_{th} described in the main text.

[1] The Polarbear Collaboration: P. A. R. Ade, Y. Akiba, A. E. Anthony, K. Arnold, M. Atlas, D. Barron, D. Boettger, J. Borrill, S. Chapman, Y. Chinone, M. Dobbs, T. Elleflot, J. Errard, G. Fabbian, C. Feng, D. Flanigan, A. Gilbert, W. Grainger, N. W. Halverson, M. Hasegawa, K. Hattori, M. Hazumi, W. L. Holzapfel, Y. Hori, J. Howard, P. Hyland, Y. Inoue, G. C. Jaehnig, A. H. Jaffe, B. Keating, Z. Kermish, R. Keskitalo, T. Kisner, M. Le Jeune, A. T. Lee, E. M. Leitch, E. Linder, M. Lungu, F. Matsuda, T. Matsumura, X. Meng, N. J. Miller, H. Morii, S. Moyerman, M. J. Myers, M. Navaroli, H. Nishino, A. Orlando, H. Paar, J. Peloton, D. Poletti, E. Quealy, G. Rebeiz, C. L. Reichardt, P. L. Richards, C. Ross, I. Schanning, D. E. Schenck, B. D. Sherwin, A. Shimizu, C. Shimmin, M. Shimon, P. Siritanasak, G. Smecher, H. Spieler, N. Stebor, B. Steinbach, R. Stompor, A. Suzuki, S. Takakura, T. Tomaru, B. Wilson, A. Yadav, and O. Zahn. A measurement of the cosmic microwave background B-mode polarization power spectrum at subdegree scales from two years of POLARBEAR data. *The Astrophysical Journal*, 794(2):171, October 2014.

[2] Mathew Madhavacheril, Neelima Sehgal, Rupert Allison, Nick Battaglia, J. Richard Bond, Erminia Calabrese, Jerod Caligiuri, Kevin Coughlin, Devin Crichton, Rahul Datta, Mark J. Devlin, Joanna Dunkley, Rolando Dünner, Kevin Fogarty, Emily Grace, Amir Hajian, Matthew Hasselfield, J. Colin Hill, Matt Hilton, Adam D. Hincks, Renée Hlozek, John P. Hughes, Arthur Kosowsky, Thibaut Louis, Marius Lungu, Jeff McMahon, Kavilan Moodley, Charles Munson, Sigurd Naess, Federico Nati, Laura Newburgh, Michael D. Niemack, Lyman A. Page, Bruce Partridge, Benjamin Schmitt, Blake D. Sherwin, Jon Sievers, David N. Spergel, Suzanne T. Staggs, Robert Thornton, Alexander Van Engelen, Jonathan T. Ward, and Edward J. Wollack. Evidence of lensing of the cosmic microwave background by dark matter halos. *Physical Review Letters*, 114(15):151302, April 2015.

[3] Duncan Farrah, Kimberly Ennico Smith, David Ardila, Charles M. Bradford, Michael Dipirro, Carl Ferkinhoff, Jason Glenn, Paul Goldsmith, David Leisawitz, Thomas Nikola, Naseem Rangwala, Stephen A. Rinehart, Johannes Staguhn, Michael Zemcov, Jonas Zmuidzinas, and James Bartlett. Review: far-infrared instrumentation and technological development for the next decade. *Journal of Astronomical Telescopes, Instruments, and Systems*, 5(02):1, April 2019.

[4] Arttu Luukanen, Roger Appleby, Mike Kemp, and Neil Salmon. Millimeter-wave and terahertz imaging in security applications. In Kai-Erik Peiponen, Axel Zeitler, and Makoto Kuwata-Gonokami, editors, *Terahertz Spectroscopy and Imaging*, pages 491–520. Springer Berlin Heidelberg, Berlin, Heidelberg, 2013.

[5] Joel N Ullom and Douglas A Bennett. Review of superconducting transition-edge sensors for X-ray and gamma-ray spectroscopy. *Superconductor Science and Technology*, 28(8):084003, July 2015.

[6] Antoni Rogalski. *Infrared and Terahertz Detectors*. Taylor & Francis Group, 2022.

[7] E. A. Grace, J. Beall, H. M. Cho, M. J. Devlin, A. Fox, G. Hilton, J. Hubmayr, K. Irwin, J. Klein, D. Li, M. Lungu, L. B. Newburgh, J. Nibarger, M. D. Niemack, J. McMahon, L. A. Page, C. Pappas, B. L. Schmitt, S. T. Staggs, J. Van Lanen, and E. Wollack. Characterization and performance of a Kilo-TES sub-array for ACTPol. *Journal of Low Temperature Physics*, 176(5):705–711, February 2014.

[8] Daniel Dutcher, Shannon M. Duff, John C. Groh, Erin Healy, Johannes Hubmayr, Bradley R. Johnson, Dante Jones, Ben Keller, Lawrence T. Lin, Michael J. Link, Tammy J. Lucas, Samuel Morgan, Yudai Seino, Rita F. Sonka, Suzanne T. Staggs, Yuhua Wang, and Kaiwen Zheng. The simons observatory: Large-scale characterization of 90/150 GHz TES detector modules. *Journal of Low Temperature Physics*, 214(3–4):247–255, February 2024.

[9] Mario De Lucia, Paolo Dal Bo, Eugenia Di Giorgi, Tommaso Lari, Claudio Puglia, and Federico Paolucci. Transition edge sensors: Physics and applications. *Instruments*, 8(4):47, October 2024.

[10] Charles Matt Bradford, Bruce Cameron, Bradley Moore, Steve Hailey-Dunsheath, Edward Amatucci, Damon Bradley, James Corsetti, David Leisawitz, Michael DiPirro, James Tuttle, Ari Brown, Dick Mc Birney, Alexandra Pope, Lee Armus, Margaret Meixner, and Klaus Pontoppidan. Origins Survey Spectrometer: revealing the hearts of distant galaxies and forming planetary systems with far-IR spectroscopy. *Journal of Astronomical Telescopes, Instruments, and Systems*, 7(01), March 2021.

[11] K. D. Irwin. An application of electrothermal feedback for high resolution cryogenic particle detection. *Applied Physics Letters*, 66(15):1998–2000, April 1995.

[12] Boris S. Karasik and Robin Cantor. Demonstration of high optical sensitivity in far-infrared hot-electron bolometer. *Applied Physics Letters*, 98(19), May 2011.

[13] T. T. Heikkilä, R. Ojaajarvi, I. J. Maasilta, E. Strambini, F. Giazotto, and F. S. Bergeret. Thermoelectric radiation detector based on superconductor-ferromagnet systems. *Physical Review Applied*, 10(3):034053, September 2018.

[14] Steven Hailey-Dunsheath, Reinier M. J. Janssen, Jason Glenn, Charles M. Bradford, Joanna Perido, Joseph Redford, and Jonas Zmuidzinas. Kinetic inductance detectors for the origins space telescope. *Journal of Astronomical Telescopes, Instruments, and Systems*, 7(01), March 2021.

[15] A. Paiella, A. Coppolecchia, L. Lamagna, P.A.R. Ade, E.S. Battistelli, M. G. Castellano, I. Colantoni, F. Columbro, G. D'Alessandro, P. de Bernardis, S. Gordon, S. Masi, P. Mauskopf, G. Pettinari, F. Piacentini, G. Pisano, G. Presta, and C. Tucker. Kinetic induc-

tance detectors for the OLIMPO experiment: design and pre-flight characterization. *Journal of Cosmology and Astroparticle Physics*, 2019(01):039–039, January 2019.

[16] Albert Wandui, James J. Bock, Clifford Frez, M. Hollister, Lorenzo Minutolo, Hien Nguyen, Bryan Steinbach, Anthony Turner, Jonas Zmuidzinas, and Roger O'Brient. Thermal kinetic inductance detectors for millimeter-wave detection. *Journal of Applied Physics*, 128(4), July 2020.

[17] Dmitri Golubev and Leonid Kuzmin. Nonequilibrium theory of a hot-electron bolometer with normal metal-insulator-superconductor tunnel junction. *Journal of Applied Physics*, 89(11):6464–6472, June 2001.

[18] Leonid Kuzmin. Ultimate cold-electron bolometer with strong electrothermal feedback. In Jonas Zmuidzinas, Wayne S. Holland, and Stafford Withington, editors, *Millimeter and Submillimeter Detectors for Astronomy II*, volume 5498, pages 349 – 361. International Society for Optics and Photonics, SPIE, 2004.

[19] L. S. Kuzmin, A. L. Pankratov, A. V. Gordeeva, V. O. Zbrozhek, V. A. Shamporov, L. S. Revin, A. V. Blagodatkin, S. Masi, and P. de Bernardis. Photon-noise-limited cold-electron bolometer based on strong electron self-cooling for high-performance cosmology missions. *Communications Physics*, 2(1), September 2019.

[20] A. Ozaeta, P. Virtanen, F. S. Bergeret, and T. T. Heikkilä. Predicted very large thermoelectric effect in ferromagnet-superconductor junctions in the presence of a spin-splitting magnetic field. *Physical Review Letters*, 112(5):057001, February 2014.

[21] G. Marchegiani, A. Braggio, and F. Giazotto. Nonlinear thermoelectricity with electron-hole symmetric systems. *Physical Review Letters*, 124(10):106801, March 2020.

[22] Heli Vora, Piranavan Kumaravadivel, Bent Nielsen, and Xu Du. Bolometric response in graphene based superconducting tunnel junctions. *Applied Physics Letters*, 100(15), April 2012.

[23] C B McKitterick, D E Prober, H Vora, and X Du. Ultra-sensitive graphene far-infrared power detectors. *Journal of Physics: Condensed Matter*, 27(16):164203, April 2015.

[24] Francesco Vischi, Matteo Carrega, Alessandro Braggio, Federico Paolucci, Federica Bianco, Stefano Roddaro, and Francesco Giazotto. Electron cooling with graphene-insulator-superconductor tunnel junctions for applications in fast bolometry. *Physical Review Applied*, 13(5):054006, May 2020.

[25] Leonardo Lucchesi and Federico Paolucci. Out-of-equilibrium nonlinear model of thermoelectricity in superconducting tunnel junctions. *Physical Review B*, 112(18), November 2025.

[26] Federica Bianco, Ding Zhang, and Federico Paolucci. Co-existence of linear and non-linear thermoelectricity in graphene-superconductor tunnel junctions. *Journal of Applied Physics*, 136(15), October 2024.

[27] Michael Tinkham. *Introduction to superconductivity*. Dover books on physics. Dover Publ., Mineola, NY, second edition, 2015.

[28] Giorgio De Simoni, Federico Paolucci, Paolo Solinas, Elia Strambini, and Francesco Giazotto. Metallic supercurrent field-effect transistor. *Nature Nanotechnology*, 13(9):802–805, July 2018.

[29] Federico Paolucci, Gaia Germanese, Alessandro Braggio, and Francesco Giazotto. A highly sensitive broadband superconducting thermoelectric single-photon detector. *Applied Physics Letters*, 122(17), April 2023.

[30] SR Golwala, J Jochum, and B Sadoulet. Noise considerations in low resistance nis junctions. In S. Cooper, editor, *Proceedings of the VIIth International Workshop on Low Temperature Detectors, 27 July–2 August, 1997, Munich, Germany*, pages 64–65, 1997.

[31] Francesco Giazotto, Tero T. Heikkilä, Arttu Luukanen, Alexander M. Savin, and Jukka P. Pekola. Opportunities for mesoscopics in thermometry and refrigeration: Physics and applications. *Reviews of Modern Physics*, 78(1):217–274, March 2006.

[32] John C. Mather. Bolometer noise: nonequilibrium theory. *Applied Optics*, 21(6):1125, March 1982.

[33] H. Nyquist. Thermal agitation of electric charge in conductors. *Physical Review*, 32(1):110–113, July 1928.

[34] Federico Paolucci, Vittorio Buccheri, Gaia Germanese, Nadia Ligato, Riccardo Paoletti, Giovanni Signorelli, Massimiliano Bitossi, Paolo Spagnolo, Paolo Falferi, Mauro Rajteri, Claudio Gatti, and Francesco Giazotto. Development of highly sensitive nanoscale transition edge sensors for gigahertz astronomy and dark matter search. *Journal of Applied Physics*, 128(19), November 2020.

[35] P. L. Richards. Bolometers for infrared and millimeter waves. *Journal of Applied Physics*, 76(1):1–24, July 1994.

[36] Ya.M. Blanter and M. Büttiker. Shot noise in mesoscopic conductors. *Physics Reports*, 336(1–2):1–166, September 2000.